Research Article | Vol. 31, No. 22 / 23 Oct 2023 / Optics Express 37011
Optics EXPRESS

Coexistence of gain-through-filtering and parametric instability in a fiber ring cavity

STEFANO NEGRINI,[1,*] JEAN BAPTISTE CEPPE,[1] MATTEO CONFORTI,[1] AURO M. PEREGO,[2] ALEXANDRE KUDLINSKI,[1] AND ARNAUD MUSSOT[1]

[1]Univ. Lille, CNRS, UMR 8523-PhLAM-Physique des Lasers Atomes et Molécules, F- 59000 Lille, France
[2]Aston Institute of Photonic Technologies, Aston University, Birmingham, B4 7ET, UK
[*]stefano.negrini@univ-lille.fr

Abstract: We experimentally and numerically investigate the dynamics of a fiber ring cavity in which two different instability can be excited: gain-through-filtering and parametric instability. We demonstrate that they can be triggered individually or collectively depending on the two main control parameters offered by the cavity, namely the pump power and the cavity detuning. The experimental observations are in good agreement with numerical simulations.

1. Introduction

Modulation instability (MI) is a well known nonlinear process consisting in the exponential amplification of phase-matched waves [1]. The phenomenon has been investigated in several fields of physics ranging from fluid dynamics [2,3], to plasma physics [4] or nonlinear fiber optics [5–10]. In fiber optics, optical resonators are a widely studied class of devices. Their structure enables a strong enhancement of nonlinear effects as well as an easy control of the parameters and a real-time monitoring of the dynamics of the processes due to their relatively low repletion rates. After the first observations of MI in passive fiber ring resonators by Nakazawa *et al.* [11] and by Coen *et al.* [12], several results have been reported including frequency comb generation [13], the competition between Turing and Faraday instabilities [14], the observation of highly nonlinear regimes in P1-P2 regimes [15], the prediction of extreme events [16] and the evidence of gain-through-filtering (GTF) process [17]. In particular for GTF, the inclusion of spectrally-localized losses is a counter-intuitive mechanism which may generate MI gain, as it was theoretically predicted [18,19] and experimentally observed [17]. Practically, an ultra-narrow optical filter located on one side of the pump carries an additional contribution to the phase-matching relation, which may render the cavity modulationally unstable. Beside the fundamental interest, GTF enables the observation of MI in any dispersion regimes and to control the MI frequency shift, which are key features for frequency comb generation in optical resonators [20]. The first observation of GTF was recently reported by Bessin *et al.* [17] in a very restricted area of parameters. The inclusion of an additional component within the cavity, such as a filter, opens the way to a richer nonlinear dynamics, which still need an experimental investigation. In this paper we report the observation of the coexistence of different instabilities by exploring a larger range of parameters. We show that, in addition to GTF, parametric instabilities [21] can be sustained inside the cavity. The power threshold of the two phenomena can be controlled by varying the cavity phase detuning, meaning that it's possible to trigger either GTF and parametric instability individually, or both simultaneously.

#498572 https://doi.org/10.1364/OE.498572
Journal © 2023 Received 21 Jun 2023; revised 31 Aug 2023; accepted 2 Sep 2023; published 18 Oct 2023

Optics EXPRESS

2. Model and parametric gain

We model the dynamics of the passive fiber cavity by the Ikeda map [22], including the effect of the filter in the boundary conditions as described in [19]:

$$i\frac{\partial A_n}{\partial z} - \frac{\beta_2}{2}\frac{\partial {A_n}^2}{\partial t^2} + \gamma|A_n|^2 A_n = 0, \quad 0<z<L, \tag{1}$$

$$A_{n+1}(z=0,t) = \theta E_{in} + \rho e^{i\phi_0} h(t) * A_n(z=L,t). \tag{2}$$

The variable A_n is the slowly varying envelope of the electric field, E_{in} is input electric field, $\beta_2 = \partial^2\beta(\omega)/\partial w^2|_{\omega=\omega_p}$ is the dispersion at the pump pulsation ω_p, γ is the nonlinear coefficient, t is the retarded time, z is the distance traveled inside the cavity and L is the cavity length. The parameter θ is the coupler transmission coefficient, while all the losses of the cavity, except the one from the filter, are lumped into ρ ($\rho^2 + \theta^2<1$). In the following we will refer to ρ as lumped loss factor. With this definition, it's possible to relate losses and cavity finesse as $F = \pi\sqrt{\rho}/(1-\rho)$ [19]. The linear phase detuning of the cavity can be expressed as $\phi_0 = \omega_p nL/c$ mod (2π), where n is the refractive index of the fiber and c the speed of light in vacuum. The function $h(t) = \mathcal{F}^{-1}[H(\omega)]$ is the impulse response of the fiber Bragg grating filter, with the transfer function defined as $H(\omega) = e^{(F(\omega)+i\psi(\omega))}$. The functions $F(\omega)$ and $\psi(\omega)$ are the loss and phase profile functions, respectively, which are related together through Kramer-Kronig relations. Specifically, by fitting the loss profile with a higher-order Lorentzian function, one can describe the phase with the following expressions [19]:

$$F(\omega) = b\frac{a^4}{(\omega-\omega_f)^4 + a^4}, \tag{3}$$

$$\psi(\omega) = ba\frac{(\omega-\omega_f)[(\omega-\omega_f)^2 + a^2]}{\sqrt{2}[(\omega-\omega_f)^4 + a^4]}, \tag{4}$$

with a and b being the fitting parameters for the loss profile, and ω_f is the central angular frequency of the filter.

By performing a linear stability analysis of the continuous wave solutions of Eq. (1), the following expression of the parametric gain is obtained [19]:

$$g_{MAP}(\omega) = 2\ln\max\{|\lambda_1|, |\lambda_2|\}/L \tag{5}$$

$$\lambda_{1,2} = \frac{\Delta}{2} \pm \sqrt{\frac{\Delta^2}{2} - W} \tag{6}$$

$$W = \rho^2(H_e^2 + H_o^2) \tag{7}$$

$$\Delta = \rho\Big[2\cos(kL)(H_e\cos\Phi - H_o\sin\Phi) - \frac{\beta_2\omega^2 + 2\gamma P}{k}\sin(kL)(H_o\cos\Phi - H_e s \in \Phi)\Big]. \tag{8}$$

In this formulation $\lambda_{1,2}$ are the eigenvalue computed from the solution of the propagation matrix obtained in the stability analysis [19], $H_e = \mathcal{F}\{Re(h(t))\}$ and $H_o = \mathcal{F}\{Im(h(t))\}$ are the even and odd parts of $H(\omega)$, $\Phi = \phi_0 + \gamma PL$ is the total phase shift of the cavity, and $k(\omega) = \sqrt{\frac{\beta_2\omega^2}{2}(\frac{\beta_2\omega^2}{2} + 2\gamma P)}$ is the wave number of the perturbation. The input power (P_{IN}) and the intracavity power (P) are related together with $P_{IN} = P[1 + \rho^2 + |H(0)|^2 - 2\rho|H(0)|cos(\phi_0 + \gamma PL + \psi(0))]/\theta^2$ [19].

Optics EXPRESS

3. Theoretical analysis

To begin our analysis, we evaluate Eq. (5) as a function of the wavelength shift between the pump and the filter, in an interval defined as $\Delta_\lambda = \lambda_p - \lambda_{Bragg}$. The result is depicted in Fig. 1(a): the 2D plot shows the parametric gain evolution from $\Delta_\lambda = -12$ nm to $\Delta_\lambda = 12$ nm. The first feature that stands out is the peculiar X shape created by the GTF bands in the interval $|\Delta_\lambda|<8$ nm. Those branches are the graphical representation of the tunable feature of GTF, already observed in [17], where the gain bands move accordingly to the relative Δ_λ between pump and filter. One can also note that GTF is not the only instability visible in the plot. Indeed, for $|\Delta_\lambda|>8$ nm, and for $-8<\Delta_\lambda<0$ nm, another couple of bands, close to ±1 THz, is clearly visible. Since the position of those bands does not depend on the relative shift Δ_λ, one can easily identify them as parametric instabilities, whose position is determined mainly by the dispersion of the cavity (which in this case is maintained constant no matter the wavelength). Interestingly, for $-8<\Delta_\lambda<0$ nm, GTF and parametric instabilities exist simultaneously, while for $0<\Delta_\lambda<8$ nm only GTF is present. This difference between the two sides is directly related to the phase of the filter described by the function $\psi(\omega)$ in Eq. (3) and shown in Fig. 3(b). Indeed, the phase is an odd function with respect to the filter central frequency: it approaches zero with an opposite sign for negative and positive frequency shift, modifying differently the phase-matching condition of the cavity. To get a clearer insight, we plotted the parametric gain at four typical Δ_λ values. Figures 1(b) and 1(e) display the parametric gain for $|\Delta_\lambda| = 10$ nm, for which the gain shows only parametric instabilities around ±1 THz. Figures 1(c) and (d) represent the gain at $\Delta_\lambda = +5$ nm and $\Delta_\lambda = -5$ nm, respectively. In Fig. 1(c) only GTF is stimulated, but in Fig. 1(d) the instabilities coexist: GTF around ±0.60 THz and parametric bands around ±1 THz. The first experimental observation of GTF [17] focused on a positive Δ_λ interval where no parametric bands were destabilized as in Fig. 1(c). There is a competition between parametric and GTF instabilities which depends on the relative position of the pump compare to the filter due to the asymmetric phase of the filter. Here, we focus on the relation between GTF and parametric instabilities for a fixed negative Δ_λ, where those two effects coexist as shown in Fig. 1(d).

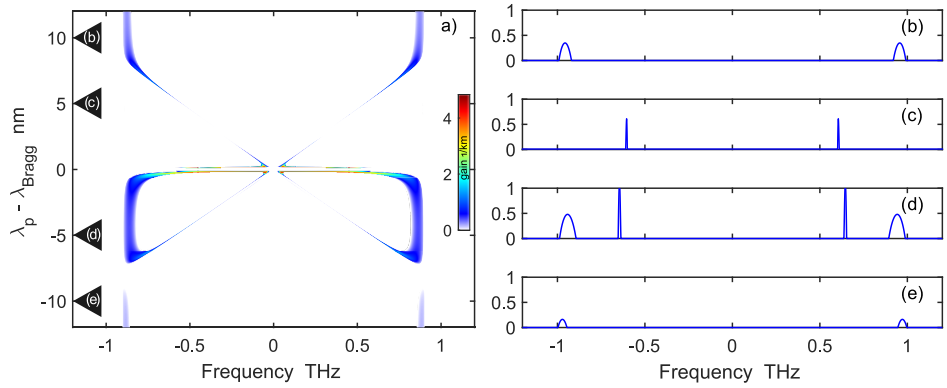

Fig. 1. (a) Evolution of the parametric gain as a function Δ_λ from Eq. (5). The parameters used for the calculation are: P_{IN}=18.5 W, ϕ_0 = 0 rad, γ = 1.05 /W/km, L=205.3 m, β_2 = 0.43 ps^2/km, $\rho = \sqrt{0.635}$ and $\theta = \sqrt{0.1}$. The central wavelength of the filter is λ_f = 1549.4 nm, with fitting parameters a = 85 rad/ns, b = −2.45. (b)-(e) Four examples of the parametric gain at Δ_λ equal to +10 nm, 5 nm, −5 nm and −10 nm respectively.

We proceed with the investigation by studying the evolution of the gain as a function of P_{IN} and linear detuning ϕ_0, under the constraint of maintaining the cavity monostable for the sake of simplicity. In Fig. 2 we display the parametric gain band, obtained from Eq. (5). Only negative frequencies are displayed, due to the symmetry of the bands. Note that the maximum of the

Optics EXPRESS

instability band does not perfectly correspond to the maximum loss of the filter as it was observed and detailed in [19]. In particular: Fig. 2(a) illustrates the evolution of the gain for $\phi_0 = 0.26$ rad, as a function of the input pump power. The blue dashed line denotes the input power threshold for parametric instabilities ($P_{IN} = 17.65$ W), and the red dashed line represents the threshold for the GTF ($P_{IN} = 18$ W) and the vertical black dashed lines highlight the central frequency of the filter. Similarly, Fig. 2(b) depicts the evolution of the gain for $\phi_0 = -0.26$ rad, blue dashed line indicating the parametric instability threshold ($P_{IN} = 13.9$ W), and the red dashed lines indicating GTF instability ($P_{IN} = 10.33$ W). For both plots it is possible to see parametric instabilities around -1 THz and GTF instabilities around -0.6 THz, but the order of appearance of the two phenomena is reversed. Indeed, if for $\phi_0 = -0.26$ rad parametric instabilities arise for lower input power with respect to GTF, for $\phi_0 = 0.26$ rad the situation is reversed. Thus we can choose to trigger one process or the other, by tuning the cavity detuning and pump power.

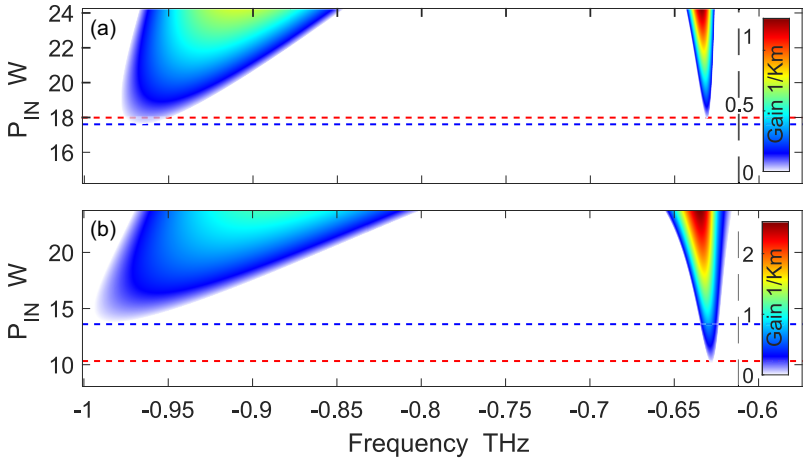

Fig. 2. Evolution of the gain as a function of the pump power at a fixed $\Delta_\lambda = 5$ nm at different phase detuning. All the parameters except ϕ_0 and P_{IN} are listed in the caption of Fig. 1. (a) Gain evolution for $\phi_0 = 0.26$ rad. (b) Gain evolution for $\phi_0 = -0.26$ rad. Red dashed lines highlight the threshold power of GTF, the blue dashed lines the threshold power for parametric instabilities, the black dashed vertical line highlights the central frequency of the filter. It is worth noting the inversion in the order of appearance of the instabilities with respect to input power at different linear phase detunings.

4. Experimental setup

Before going into the details of our results, we proceed with the description of the experimental setup used displayed in Fig. 3(a). The cavity is structured as follows: $L_f = 203$ m of dispersion shifted fiber, one 90/10 injection fiber coupler, one 95/5 tap fiber coupler, and the FBG filter. The couplers, having a total length of $L_c = 1.8$ m, are chosen to be normally dispersive at the wavelength of the pump, whilst the FBG is engraved on $L_{FBG} = 0.5$ m of standard SMF28 optical fiber. The total length of the cavity is thus $L = L_f + L_c + L_{FBG} = 205.3$ m, with an average dispersion of $\beta_2 = 0.43$ ps ^{2}/km and a nonlinear coefficient $\gamma = 1.05$/W/km. The FBG has a central wavelength $\lambda_{Bragg} = 1549.44$ nm (193.49 THz) and a FWHM of 0.29 nm (30 GHz), see Fig. 3(b). The finesse of the cavity is $F = 14$ corresponding to a lumped loss factor $\rho = \sqrt{0.635}$. The pump is a cw laser centered at $\lambda_p = 1544.4$ nm. The pump is split into two beams with an optical 90/10 coupler: 90 % of the power is used as *nonlinear* beam (red) which coherently drives the cavity, while the remaining 10 % is used as *control* beam (blue) to stabilize the cavity.

Optics EXPRESS

The *nonlinear* beam is modulated into flat-top pulses with an intensity electro-optical modulator (EOM) and then processed with an acousto-optic modulator (AOM). The two modulators are used to create a train of pulses: the EOM is used to generate a flat-top optical pulsed signal, with a duration of 1 ns and a period of 1.06 μs. The AOM is driven by a gated-sinusoidal signal and serves a double purpose. Firstly, a gating function, synchronized with the pulses of the EOM, allows to enhance the extinction ratio of the train of pulses up to 50 dB to avoid stimulated-Brillouin-scattering. Secondly, it superimposes a sinusoidal signal upon the pulses, allowing for a fine control of the phase detuning ϕ_0. We remind for clarity that the relation between the phase detuning ϕ_0 and the pump frequency ω_p is $\phi_0 = \omega_p nL/c$. The pulses are amplified through an erbium doped fiber amplifier (EDFA1) and polarization is aligned with a paddle (PC1) [12], before being fed into the cavity through the 90/10 injection coupler. In this work the effects of the polarization are not studied but, for an optimal level of intracavity power, we make sure that the polarization of the input field is well aligned with one of the polarization axis of the cavity. The *control* beam path consists of a phase modulator (PM), an erbium doped amplifier (EDFA2) and a paddle (PC2). The phase modulator (PM) is part of the stabilization scheme, together with the Pound-Drever-Hall (PDH) [23] and the PID modules. The amplifier EDFA2 is used to compensate for the losses of the two modulators.

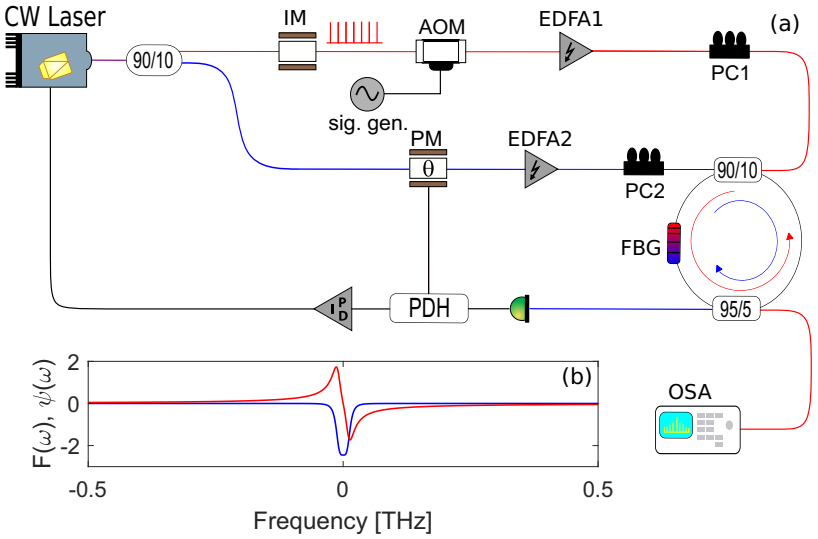

Fig. 3. (a) Experimental setup. EOM: electro-optical intensity modulator, PM: optical phase modulator, AOM: acusto-optical frequency modulator, EDF1-2 : Erbium-doped Fiber Amplifiers, PC1-2: Polarization controllers, PDH: Pound-Drever-Hall controller, PID: proportional-integrative-derivative controller, FBG: fiber Bragg grating. (b) Filter transfer function modulus $|H(\omega)|$ in blue and phase $\psi(\omega)$ in red. The plot is centered on the frequency of the pump.

5. Experimental results

As the first result, we compare the measured output spectra for two cavity phase detunings with numerical simulations of Eq. (1) performed with a split-step Fourier method. The parameters of the cavity are listed in the caption of Fig. 1, except for the linear detuning and the input power, which vary accordingly to the measurements. Fig. 4(a) illustrates the spectrum at $\phi_0 = -0.26$ rad for $P_{IN} = 14.1$ W, while in Fig. 4(b) $P_{IN} = 18$ W. For both figures red traces are the experimental measurements, and blue traces are the simulated spectra. We also plot the profile of the filter in

Optics EXPRESS

yellow, as a reference for the bands position. One can note that in Fig. 4(a), the spectrum displays only GTF components with the first band at ±0.61 THz. Figure 4(b) shows that increasing the input power leads to the appearance of parametric instability bands at ±0.97 THz. In the latter case, it's also possible to note some spurious spectral components at ±0.36 THz, due to four-wave-mixing. The frequency of those components is simply the difference between the GTF and parametric instabilities frequencies. One can note that the numerical simulations and the measurements are in good agreement.

Figure 5(a) reports a plot of the spectrum at $\phi_0 = 0.26$ rad for $P_{IN} = 21$ W, and Fig. 5(b) for $P_{IN} = 26$ W. The color code of the traces is the same as Fig. 4. In Fig. 5(a), firstly we can see the appearance of parametric instabilities at 0.95 THz, followed at higher powers by GTF instabilities at 0.57 THz as depicted in Fig. 5(b). As the previous case, the coexistence of the two instabilities leads to the formation of spurious components at ±0.38 THz. Again, numerical simulations and measurements are in very good agreement, for both position of the bands and the order of appearance. It is important to note that the predictions of the analytical model (Eq. (5)) are in qualitative agreement with these results. It indeed predicts the order of appearance of the instabilities (see Fig. 2), but there is no quantitative agreement concerning the threshold values because it assumes a uniform cavity while we used different fiber type to set the average dispersion of the cavity to slightly normal value. We observed numerically the threshold values are slightly modified due to the dispersion management within the cavity. Finally, we illustrate the overall evolution of the threshold of parametric and GTF instabilities as a function of the linear cavity detuning ϕ_0. Figure 6 represent the evolution of the parametric (blue) and GTF (red) threshold evolution from analytical (Eq. (5), Fig. 6(a)) and numerical (Eq (1), Fig. 6(b)) predictions, vs experiments (Fig. 6(c)). First of all we have a pretty good qualitative agreement between theoretical predictions (Figs. 6(a) and (b)) and experimental results (Fig. 6(c)). For low cavity detuning values, GTF instabilities appear first while for large ones these are parametric ones. The agreement between numerical simulations and experiments is pretty good provided that there are no free parameters in this complex system made of a large number of parameters and that the threshold can be affected by noise, slight fluctuations of the stabilization system, or drifts of the synchronization mismatch. The analytical model, while assuming a uniform cavity, provides a very good qualitative description of the dynamics of the system and can be used as toy model to get a rapid physical insight of the process.

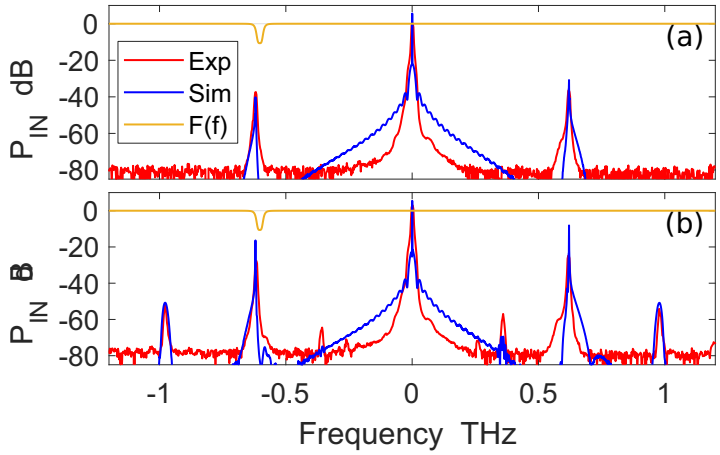

Fig. 4. Output spectra for different input powers and $\phi_0 = -0.26$ rad. (a) Spectrum for $P_{IN} = 14.1$ W, (b) Spectrum for $P_{IN} = 18$ W. Blue lines are the experimental traces, red lines are the numerical simulations. P_{IN} refers to the power used in the numerical simulations.

Optics EXPRESS

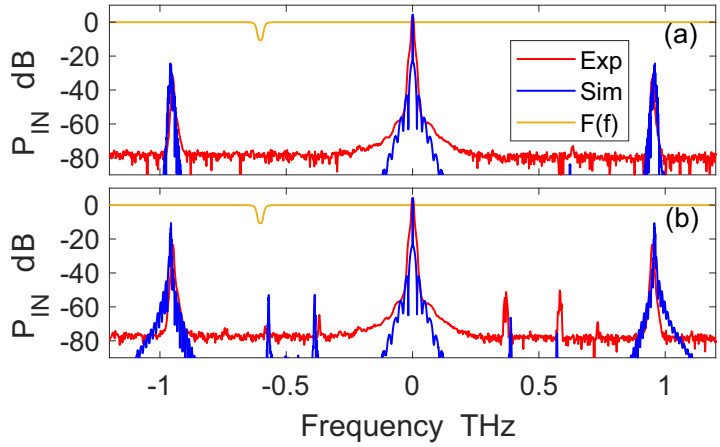

Fig. 5. Output spectra for different input powers and $\phi_0 = 0.26$ rad. (a) Spectrum for $P_{IN} = 21$ W, (b) Spectrum for $P_{IN} = 26$ W. Blue line are the experimental traces, red lines are the numerical simulations. P_{IN} refers to the power used in the numerical simulations.

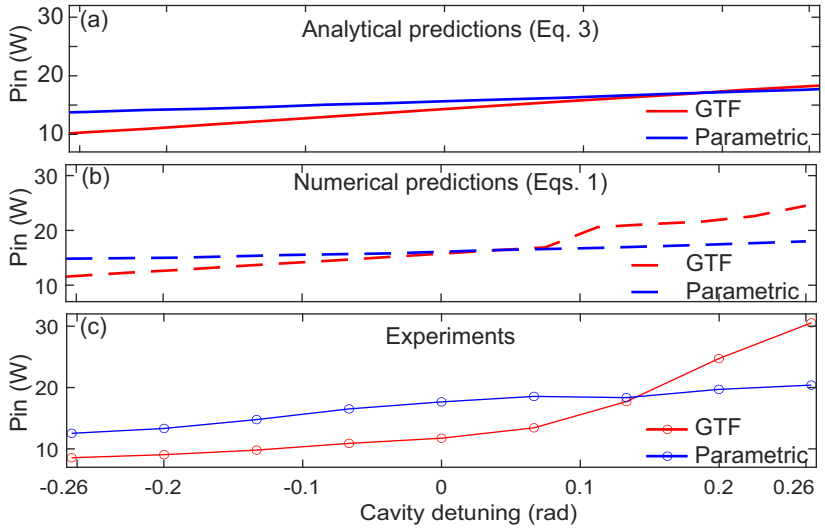

Fig. 6. Evolution of the power thresholds of the two gains as a function of the detuning ϕ_0. (a) shows the theoretical threshold evolution, computed by solving Eq. (5) as a function of power for each fixed phase detuning. (b) shows the experimental threshold evolution, recorded by changing the power at each phase detuning.

6. Conclusions

In conclusion, we have theoretically and experimentally characterised the coexistence of GTF and parametric instabilities in a fiber ring cavity. In particular, we analysed and measured the behavior of the power thresholds of GTF and parametric instability, and demonstrated how it's possible to modify the nature of the spectra by simply changing the linear phase detuning. We obtained a good agreement between experimental results and numerical simulations, confirming these observations. This study helps to complete the analysis on GTF phenomenon, and gives a more in-depth analysis on how it can interact with other common instabilities, extending the knowledge of previous studies on the topic [17].

Optics EXPRESS

Funding. Horizon 2020 Framework Programme (No 861152).

Acknowledgment. A.M.P. acknowledges support from the EPSRC project EP/W002868/1, and from the Royal Academy of Engineering through the Research Fellowship scheme.

Disclosures. The authors declare no conflicts of interest.

Data availability. Data underlying the results presented in this paper are not publicly available at this time but may be obtained from the authors upon reasonable request.

References

1. V. E. Zakharov and L. A. Ostrovsky, "Modulation instability: The beginning," Phys. D **238**(5), 540–548 (2009).
2. T. B. Benjamin and J. E. Feir, "The disintegration of wave trains on deep water Part 1. Theory," J. Fluid Mech. **27**(3), 417–430 (1967).
3. V. E. Zakharov, "Stability of periodic waves of finite amplitude on the surface of a deep fluid," J. Appl. Mech. Tech. Phys. **9**(2), 190–194 (1972).
4. B. Ghosh and K. P. Das, "Modulational instability of electron plasma waves in a cylindrical wave guide," Plasma Phys. Control. Fusion **27**(9), 969–982 (1985).
5. A. Hasegawa and W. Brinkman, "Tunable coherent IR and FIR sources utilizing modulational instability," IEEE J. Quantum Electron. **16**(7), 694–697 (1980).
6. D. Anderson and M. Lisak, "Modulational instability of coherent optical-fiber transmission signals," Opt. Lett. **9**(10), 468 (1984).
7. A. Hasegawa, "Generation of a train of soliton pulses by induced modulational instability in optical fibers," Opt. Lett. **9**(7), 288 (1984).
8. G. P. Agrawal, "Modulation instability induced by cross-phase modulation," Phys. Rev. Lett. **59**(8), 880–883 (1987).
9. S. Wabnitz, "Modulational polarization instability of light in a nonlinear birefringent dispersive medium," Phys. Rev. A **38**(4), 2018–2021 (1988).
10. P. Drummond, T. Kennedy, J. Dudley, R. Leonhardt, and J. Harvey, "Cross-phase modulational instability in high-birefringence fibers," Opt. Commun. **78**(2), 137–142 (1990).
11. M. Nakazawa, K. Suzuki, and H. A. Haus, "Modulational instability oscillation in nonlinear dispersive ring cavity," Phys. Rev. A **38**(10), 5193–5196 (1988).
12. S. Coen and M. Haelterman, "Modulational Instability Induced by Cavity Boundary Conditions in a Normally Dispersive Optical Fiber," Phys. Rev. Lett. **79**(21), 4139–4142 (1997).
13. F. Leo, S. Coen, P. Kockaert, S.-P. Gorza, P. Emplit, and M. Haelterman, "Temporal cavity solitons in one-dimensional Kerr media as bits in an all-optical buffer," Nat. Photonics **4**(7), 471–476 (2010).
14. F. Copie, M. Conforti, A. Kudlinski, A. Mussot, and S. Trillo, "Competing Turing and Faraday Instabilities in Longitudinally Modulated Passive Resonators," Phys. Rev. Lett. **116**(14), 143901 (2016).
15. F. Bessin, F. Copie, M. Conforti, A. Kudlinski, A. Mussot, and S. Trillo, "Real-time characterization of period-doubling dynamics in uniform and dispersion oscillating fiber ring cavities," Phys. Rev. X **9**(4), 041030 (2019). Publisher: American Physical Society.
16. F. Selmi, S. Coulibaly, Z. Loghmari, I. Sagnes, G. Beaudoin, M. Clerc, and S. Barbay, "Spatiotemporal chaos induces extreme events in an extended microcavity laser," Phys. Rev. Lett. **116**(1), 013901 (2016).
17. F. Bessin, A. M. Perego, K. Staliunas, S. K. Turitsyn, A. Kudlinski, M. Conforti, and A. Mussot, "Gain-through-filtering enables tuneable frequency comb generation in passive optical resonators," Nat. Commun. **10**(1), 4489 (2019).
18. A. Perego, N. Tarasov, D. Churkin, S. Turitsyn, and K. Staliunas, "Pattern Generation by Dissipative Parametric Instability," Phys. Rev. Lett. **116**(2), 028701 (2016).
19. A. M. Perego, A. Mussot, and M. Conforti, "Theory of filter-induced modulation instability in driven passive optical resonators," Phys. Rev. A **103**(1), 013522 (2021).
20. A. Pasquazi, M. Peccianti, L. Razzari, D. J. Moss, S. Coen, M. Erkintalo, Y. K. Chembo, T. Hansson, S. Wabnitz, P. Del'Haye, X. Xue, A. M. Weiner, and R. Morandotti, "Micro-combs: A novel generation of optical sources," Phys. Rep. **729**, 1–81 (2018).
21. M. Conforti, F. Copie, A. Mussot, A. Kudlinski, and S. Trillo, "Parametric instabilities in modulated fiber ring cavities," Opt. Lett. **41**(21), 5027 (2016).
22. K. Ikeda, "Multiple-valued stationary state and its instability of the transmitted light by a ring cavity system," Opt. Commun. **30**(2), 257–261 (1979).
23. E. D. Black, "An introduction to Pound–Drever–Hall laser frequency stabilization," Am. J. Phys. **69**(1), 79–87 (2001).